THE DESIGN OF A HYBRID PHOTOINJECTOR FOR HIGH BRIGHTNESS BEAM APPLICATIONS

David Alesini, Massimo Ferrario, Valeria Fusco, Bruno Spataro (INFN/LNF, Frascati (Roma))
Luca Ficcadenti, Andrea Mostacci, Luigi Palumbo (Rome University La Sapienza, Roma)
Brendan O'Shea, James Rosenzweig, Gil Travish (UCLA, Los Angeles, California)

Abstract

In this paper, we illustrate the electromagnetic and beam dynamics design procedure of a new class of photoinjector, a hybrid standing/traveling wave structure. In this device a standing wave RF gun section is integrated with a downstream traveling wave structure through a coupling cell that feeds simultaneously the two sections. We discuss the advantages in RF and beam performance of the hybrid photoinjector compared to conventional systems. The electromagnetic design has been performed using the 3D electromagnetic code HFSS. Results of beam dynamics simulations in different operating conditions are also discussed.

INTRODUCTION

The most prevalent photoinjector design in use today employs an arrangement of two accelerating structures: a standing wave (SW) gun and a post accelerating linac. The two structures are fed independently and, since the SW structure reflects nearly all of the input power at the beginning of the RF fill process, circulators and isolators need in order to protect the RF power source. A considerable interest exists for the implementation of compact photoinjectors that can produce low emittance beam with energies in the 20-30 MeV range and are scalable to high frequency. The hybrid structure (HS) that we have designed for this purpose is shown in Figure 1. It begins at the upstream end with the SW RF gun section in the initial cells, which is coupled on-axis to the RF power that is fed from the waveguide into the structure through a standard traveling wave (TW) coupling cell. This coupling cell also serves as the initial cell of a downstream TW linac section. The main advantages of this device are that:

a) this scheme serves to nearly eliminate impedance mismatches, and therefore reflected RF power, both during and after the RF filling of the SW section; the near complete removal of the transient RF reflected power allows scaling to high frequency where circulators and isolators are more difficult to construct;
b) the device requires a much simpler high power RF system than a split photoinjector: there is one klystron only and waveguide sections, attenuators, and phase shifters are avoided;
c) the device is much more compact than a split system;
d) since, for beam dynamics reasons, lower gradient can be used in the SW section, it is possible to scale the design at high frequency (without reaching intolerable field gradients);
e) the acceleration dynamics are robust, allowing flexibility in operating energy by simply changing RF power and laser injection parameters;
f) the HS avoids the bunch lengthening observed after the exit of the SW gun during the drift in a split photoinjector;
g) a simpler system allows a more feasible approach to turn-key operation;
h) the TW section will be more straightforward to fabricate than a long SW accelerator.

In the first part of the paper we illustrate the general procedure to design the HS. In particular we will discuss the results of the electromagnetic simulations obtained with HFSS [1]. In the second part of the paper we illustrate the results on beam dynamics simulations.

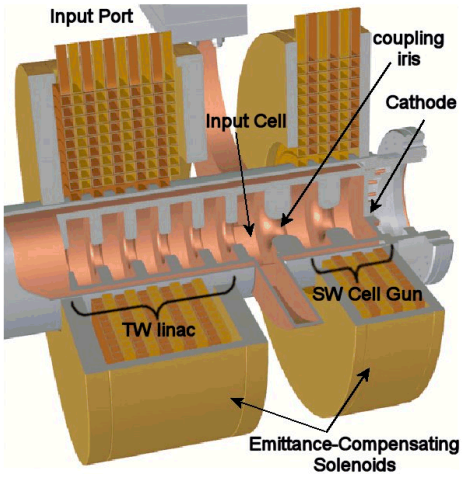

Figure 1: 3D drawing of the compact hybrid structure.

HYBRID PHOTOINJECTOR RF DESIGN

The structure can be divided in two main parts: the SW and the TW sections. In the ideal case they are divided by a perfect magnetic plane in the center of the coupling iris (see fig. 1) corresponding to the zero crossing of the longitudinal electric field. As a consequence it is possible to design the two structures separately with a perfect magnetic plane in the center of the coupling iris in order to achieve a uniform field flatness of the longitudinal electric field (E_z) in the SW gun and a zero reflection coefficient at the waveguide input port of the TW section, at the working frequency of the whole system. The final tuning of the HS can be done after this first step assembling the two parts and slightly adjusting the SW cell dimensions to perfectly tune the SW gun on resonance. It should be pointed out that, in principle, the coupler cell length and the coupling iris dimensions

(diameter and thickness) should be chosen in order to have, simultaneously, the desired ratio between the maximum amplitudes of E_z in the SW and TW sections (E_{z_SW}/E_{z_TW}) and the correct E_z phase seen by the accelerated particles. In our design we have considered a 1.6 cell SW gun and $2\pi/3$ mode accelerating TW structure and we have tuned the HS using HFSS whose 3D model is shown in Fig. 2.

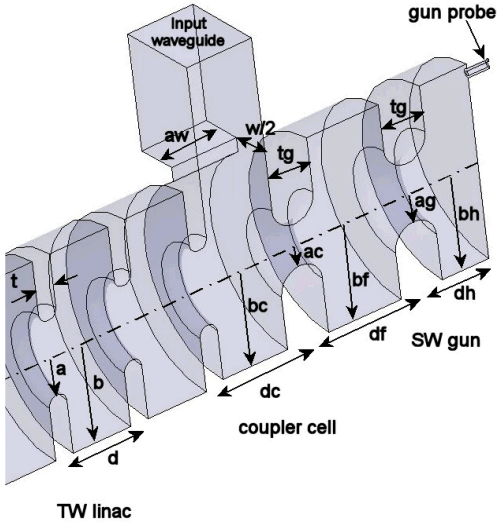

Figure 2: HFSS 3D model of the HS.

Properties of the electromagnetic field in the HS

The accelerating field in the structure can be written in the general form as:

$$E_z(z,t) = E_0(z)\cos\left(Ph_E(z) + \omega_{RF} t\right)$$

where $E_0(z)$ and $Ph_E(z)$ are the complex amplitude and phase of the accelerating field. There are several properties of E_z that can be summarized as follows:

a) the phase difference between the full cell of the SW gun and those of the input coupler cell does not depend on the geometry of the input coupler cell and iris dimensions and is about 90 deg. Typical E_0 and Ph_E profiles are shown in fig. 3 as a function of the longitudinal coordinate. The result is referred to an HS operating at 2.856GHz tuned using HFSS but can be easily generalized to other working frequencies. This result could be justified with an equivalent circuit model of the structure;

b) the coupling iris diameter allows adjusting the ratio E_{z_SW}/E_{z_TW}: in particular if we increase the diameter we increase this ratio;

c) for values of the ratio E_{z_SW}/E_{z_TW} up to 5 the perturbation on the matching of the waveguide input port with respect to the situation without SW gun is completely negligible. This is shown in Fig. 4 where the reflection coefficient at the input port of the structure is plotted with and without the SW structure. In the same plot the transmission coefficient between the gun probe and the waveguide input port is also reported.

Since E_z phase between the SW gun and the TW section is fixed, the accelerating field and the beam can be synchronized by properly choosing the length of the input coupler cell (dc). In particular with $dc = 2/3\lambda_{RF}$ the beam enter in the TW section exactly on crest while with $dc = 5/12\lambda_{RF}$ the bunch enter in the TW section on the slope of the E_z and it can be longitudinally compressed using the velocity bunching technique [2]. We call the first option continuous acceleration (CA) and the second one velocity bunching acceleration (VB). In table 1 we report the main dimensions of the two structures referred to Fig.2.

Table 1: main dimensions in mm of the HSs.

Dim	CA	VB	Dim.	CA	VB
dc	69.98	43.74	aw	36.07	30.21
df	52.48	52.48	w	33.3	35.2
dh	31.48	31.48	a	16	16
d	34.99	34.99	b	42.89	42.89
bc	40.53	40.93	ag	12.5	12.5
bf	41.66	41.7	ac	9	9
bh	41.65	41.67	tg	19.05	19.05

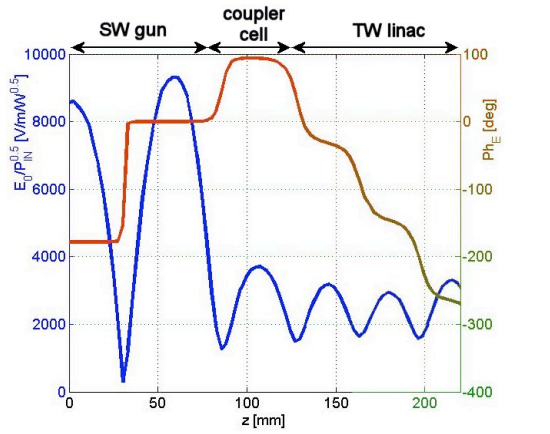

Figure 3: typical plot of E_z in the HS (HFSS simulation).

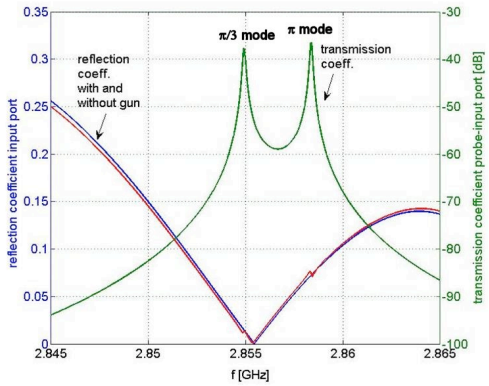

Figure 4: S_{11} at the waveguide input port and S_{21} between the gun probe and the waveguide input port

The phase between the SW and the TW structures has a high sensitivity to the resonant frequency of the SW structure itself, as shown in Fig. 5a where $Ph_E(z)$ has been plotted for different resonant frequencies of the SW gun. In the same figure the amplitude of the accelerating field

$E_0(z)$ is also reported. This sensitivity requires very good temperature stabilization of the SW section since ~0.5deg/kHz corresponds to ~22 deg/°C. On the other hand, with good temperature control, it is possible to tune the phase difference between the two structures optimizing the photoinjector performances during operation without changing the amplitudes of the accelerating field.

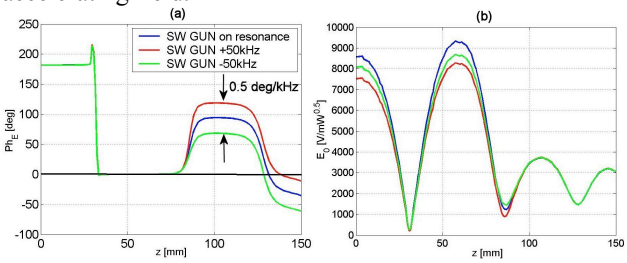

Figure 5: (a) E_0 and (b) $P\,h_E$ as a function of the longitudinal position for different resonant frequencies of the SW gun.

BEAM DYNAMICS SIMULATION

Beam dynamics simulations have been done in both cases of CA and VB using the PARMELA [3] and HOMDYN [4] codes. The amplitude of the E_{z_SW}, E_{z_TW} accelerating fields, the solenoid field in the SW and TW structures (B_{z_SW}, B_{z_TW}) and the laser input phase have been optimized to maximize the brillance of the beam at the end of the structure. The results of preliminary simulations in term of beam energy, normalized emittance, energy spread and bunch length along the structure are reported in the Figs. 6-7 for the case CA and VB respectively, using the parameters reported in table 2. The beam parameters at the end of the HSs are summarized in table 3.

Table 2: Parameters of HS beam dynamics simulations.

Parameter	CA	VB
Charge [nC]	1	1
Laser pulse length [ps]	10	10
Laser spot size radius [mm]	1.6	1.6
Total length of the HS [m]	2.2	3.1
B_{z_SW} [T]	0.2	0.15
B_{z_TW} [T]	0	0.05
$E_{z\_SW\_acc}$ ($E_{z\_SW\_peack}$) [MV/m]	35 (70)	35 (70)
$E_{z\_TW\_acc}$ ($E_{z\_TW\_peack}$) [MV/m]	13.5 (18)	13.5 (18)

Table 3: Beam parameters at the end of the HS.

Parameter	CA	VB
Rms norm emittance [mm mrad]	1.8	3.3
Energy [MeV]	31	19
Energy spread [%]	0.8	2.6
Rms bunch length [mm]	0.95	0.14

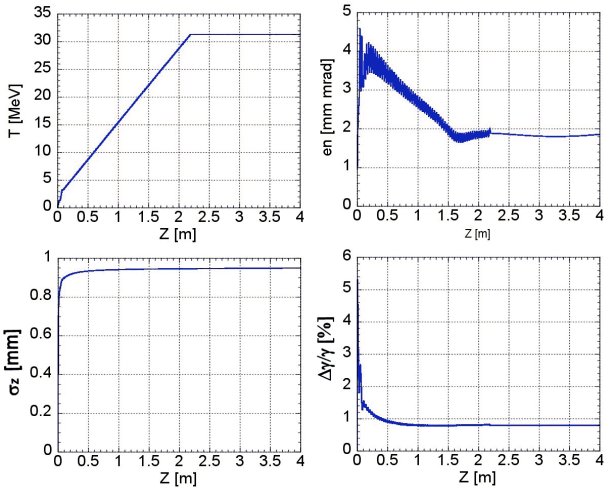

Figure 6: Beam parameters along the HS CA structure.

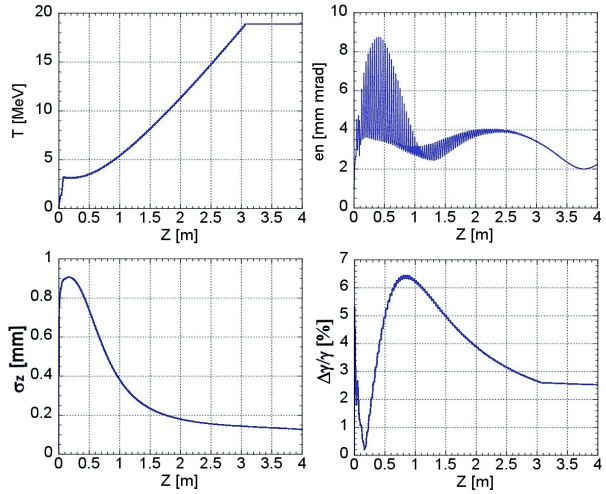

Figure 7: Beam parameters along the HS VB structure.

CONCLUSIONS

We illustrated the electromagnetic and beam dynamics design procedure of a new class of photoinjector, a hybrid standing/traveling wave structure. There are several advantages in RF and beam performance of this system compared to conventional systems: no impedance mismatch both during and after the RF filling of the SW section, much simpler high power RF system than a split photoinjector, compactness, lower RF gradient, ecc. Two different structures have been designed for acceleration and velocity bunching. The beam energies are in the range of 20-30 MeV while the norm. emittances between 2-3 mm·mrad, according to simulations. Bunch length of 0.15 mm can be reached in the velocity bunching design while the energy spread is below 3%.

REFERENCES

[1] www.ansoft.com.
[2] L.Serafini, M.Ferrario, AIP Conf. Proc. No 581, 2001.
[3] J. Billen, "PARMELA", LA-UR-96-1835, 1996.
[4] M. Ferrario et al., SLAC-PUB-8400.